LULEÅ TEKNISKA UNIVERSITET

2000:157

MASTER'S THESIS

Influence of Carbon Dioxide on the Kinetics of the Reaction between Sodium Carbonate and Sodium Trititanate

Maria Edin

Civilingenjörsprogrammet

Institutionen för Kemi och metallurgi
Avdelningen för Kemisk apparatteknik

2000:157 • ISSN: 1402-1617 • ISRN: LTU-EX--00/157--SE

ABSTRACT

A promising method for the recovery of the pulping chemicals at kraft pulp mills is the direct causticization. In this process, a gasifier and a titanate cycle replace the conventional recovery boiler and lime cycle. The aim of this study was to investigate the influence of carbon dioxide on the reaction kinetics for the solid state reaction between sodium carbonate and sodium trititanate, i.e. the direct causticization reaction occurring in the gasifier in this process.

Experiments were carried out at five different temperatures (800-880°C) and with five different amounts of carbon dioxide in the inlet gas (0-5%) in a differential reactor made of quartz glass. Kinetic data was obtained by measuring the release of carbon dioxide during the reaction. Different kinetic models were used to describe the conversion. The Valensi-Carter model describes reactions controlled by diffusion in the solid material and the phase-boundary model describes reactions controlled by chemical kinetics for a first-order reaction. Furthermore, a model including both diffusion in the solid material and chemical kinetics, the "modified shrinking-core" model, was used.

It was found that higher temperatures decrease the time to reach complete conversion. This was found for all carbon dioxide concentrations. Differences could also be seen between experiments with and without carbon dioxide, but no clear differences were seen for different amounts of carbon dioxide.

The change of controlling reaction mechanism occurred at different temperatures for different amounts of carbon dioxide in the inlet gas. When fitting the models to experimental data in the whole conversion interval it was found that the reaction was controlled by diffusion for all amounts of carbon dioxide at low temperatures. Though, when the carbon dioxide concentration in the reaction atmosphere was increased, the change of reaction mechanism to chemical kinetics occurred at higher temperatures. However, when there was carbon dioxide in the reaction atmosphere none of the models could give a good visual description in the whole conversion interval even if reasonably good standard deviation between the models and the experimental data was obtained. When the phase boundary model was fitted to the experimental data in the conversion range 8-73%, it could describe the data very well both visually and by the standard deviation calculations, which indicate that the reaction is controlled by chemical kinetics in the beginning of the reaction.

Keyword: Kraft recovery, direct causticization, titanates, carbon dioxide, kinetics, solid state reaction

PREFACE

This master thesis is the final work of the Master of Science program in Chemical Engineering at Luleå University of Technology, LTU, in Luleå, Sweden.

The laboratory work was performed at the department of Forest Products and Chemical Engineering at Chalmers University of Technology in Gothenburg, Sweden, and the rest of the study was performed at the division of Chemical Engineering Design at Luleå University of Technology in Luleå, Sweden.

I would specially like to say thank you to Lic. Eng. Ingrid Nohlgren, who has supervised this study, for all the reading she has endured and all the time she has spent helping me out!

I would also thank Lic. Eng. Peter Sedin, the examiner of this thesis, for his help and for the chair…

Furthermore, I would express my appreciation to all my colleagues at department of Chemical and Metallurgical Engineering at LTU and to everyone who helped me during my stay in Gothenburg.

Last but not least, I would like to thank Professor Hans Theliander for being a good source of knowledge and ideas.

Luleå, June 2000

Maria Edin

CONTENTS

1 INTRODUCTION

The conventional kraft pulping and recovery process is the dominating chemical recovery process at pulp mills nowadays. Black liquor is combusted in a recovery boiler and a smelt is formed, which is dissolved in a smelt dissolver yielding green liquor. The green liquor is causticized and white liquor, i.e. the pulping liquor used in the pulping unit, is formed. The conventional recovery process gives satisfactory recycling of chemicals, but it has a number of drawbacks. Some of the goals of the searching for alternative processes, which the industry has done for more than 25 years, have been to find a more efficient process with higher electricity/steam ratio and white liquor of higher quality.

One promising concept is the titanate process where a gasifier and a titanate cycle replace the recovery boiler and the lime cycle. This method is also called direct causticization because the sodium carbonate, Na_2CO_3, in the black liquor is causticized directly in the gasifier. Sodium carbonate reacts with recycled sodium trititanate, $Na_2O{\cdot}3TiO_2$, or titanium dioxide, TiO_2, from a make-up stream, yielding one solid stream mainly consisting of sodium pentatitanate, $4Na_2O{\cdot}5TiO_2$, and one gaseous stream mainly consisting of hydrogen sulphide, H_2S, and carbon dioxide, CO_2. The gaseous stream is scrubbed in an H_2S-absober and the solid stream is mixed with water in the leaching plant, yielding sodium hydroxide, NaOH, and sodium trititanate. One advantage with this process is that two streams of white liquor can be obtained; one with low sulphidity from the leaching plant and one with high sulphidity from the H_2S-absorber. Therefore, the white liquor can be tailor-made.

The characteristics and economy of this process is dependent on the causticization reactions. Therefore, it is important to understand the mechanisms of these reactions. Earlier, the temperature dependence for the reaction between sodium carbonate and sodium trititanate has been studied in a nitrogen atmosphere (Nohlgren, 1999). In a commercial gasifier, when black liquor is gasified, the gas mixture will be more complex and will consist of, for example, some carbon dioxide. Therefore, in this work, the influence of carbon dioxide concentration on the reaction rate for the reaction between sodium carbonate and sodium trititanate has been studied. Furthermore, three different mathematical reaction models were used trying to describe the reaction rate.

2 DESCRIPTION OF THE PROCESS

2.1 The Conventional Chemical Recovery Process for Kraft Black Liquor

The major chemical pulping process is the kraft pulping process, shown in Figure 2.1.

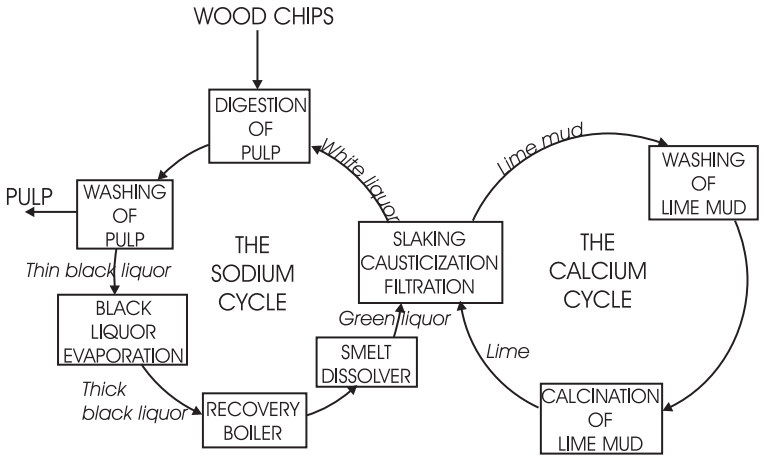

Figure 2.1. A schematic drawing of the kraft pulping and recovery process.

In the first step of the production of pulp, lignin and other organic compounds are dissolved and the cellulose fibres are uncovered, this is done in the pulp digester. The dissolving agent is white liquor, an alkaline solution where the active ions are hydroxide and hydrogensulphide, and the counterion is sodium. After this step, the lignin and the spent pulping chemicals are separated from the cellulose fibres in the pulp washing unit. The washed pulp is transported to the paper mill either directly or via a bleaching plant. The liquid leaving the washing plant is called thin black liquor and contains combustible wood substances, which can be combusted to generate steam, as well as sodium and sulphur from the white liquor, which can be used to produce new white liquor. Before combustion most of the water must be removed. This is done in the evaporation plant, yielding thick black liquor. The thick black liquor is combusted in the recovery boiler and the heat released is used to produce superheated steam. In addition, the sodium compounds are converted into sodium carbonate, Na_2CO_3, and sodium sulphide, Na_2S.

In the bottom of the recovery boiler, the inorganic chemicals form a salt smelt, which is collected and dissolved in a smelt dissolver. The liquid obtained from the

smelt dissolver is called green liquor. The green liquor contains some solid material, which is removed by filtration or sedimentation. The green liquor is then mixed with lime, CaO, and the slaking reaction (Reaction 2.1) occurs. As soon as slaked lime, $Ca(OH)_2$, forms, the causticization reaction (Reaction 2.2) starts and white liquor, NaOH, and lime mud, $CaCO_3$, are obtained.

The slaking reaction:

$$CaO\,(s) + H_2O \leftrightarrow Ca(OH)_2\,(s) \qquad (2.1)$$

The causticization reaction:

$$Ca(OH)_2\,(s) + Na_2CO_3\,(aq) \leftrightarrow 2NaOH\,(aq) + CaCO_3\,(s) \qquad (2.2)$$

The white liquor formed is separated from the lime mud by filtration and recycled to the digester. The separated lime mud is washed with water in the lime mud washing unit and then dried and calcinated (Reaction 2.3) in the lime kiln to form lime, which is recycled to the slaker. The calcination step is the main consumer of external fuel in the kraft pulp process.

The calcination reaction:

$$CaCO_3\,(s) \rightarrow CaO\,(s) + CO_2\,(g) \qquad (2.3)$$

Although, this process is the chemical recovery process used today at pulp mills all over the world, it has a number of drawbacks:

- The lime kiln is the main consumer of external fuel in a kraft pulp mill.
- Due to the equilibrium of the causticization reaction, there is a substantial dead load of sodium carbonate in the process. This dead load increases the energy demand in e.g. the digester, evaporator and recovery boiler.
- There is a smelt explosion risk when the salt smelt from the recovery boiler is dissolved.
- The heat released in the recovery boiler is recovered as steam only.

2.2 Direct Causticization of Kraft Black Liquor

One promising concept as an alternative to the conventional black liquor recovery process is the direct causticization of kraft black liquor process (Figure 2.2). In this process a gasifier, a fluidized bed or an entrained flow reactor, replaces the recovery boiler and the conventional lime cycle is replaced by a titanate cycle with direct causticization in the gasifier. In the titanate cycle, sodium carbonate in the black liquor, Na_2CO_3, reacts with added titanium dioxide, TiO_2, or recycled sodium trititanate, $Na_2O{\cdot}3TiO_2$, to form solid sodium pentatitanate, $4Na_2O{\cdot}5TiO_2$ and

carbon dioxide, CO_2. The temperature should be above 840°C in order to achieve sufficiently high reaction rates (Zou, 1991). At these high temperatures, the sodium titanates produced are still in solid form, which prevents smelt formation (Backman and Salmenoja, 1994).

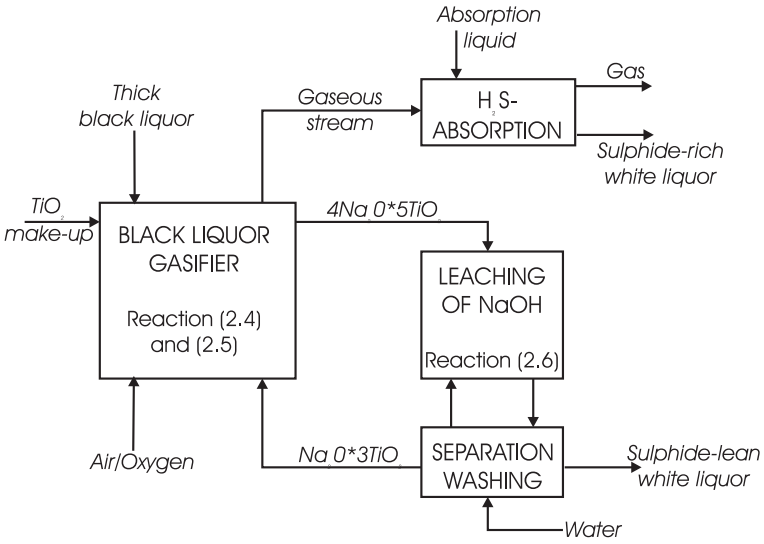

Figure 2.2. A kraft black liquor gasification process with direct causticization in the gasifier.

There are three main reactions involving titanates in the recovery process based on sodium titanate, Reaction (2.4) to (2.6), where Reaction (2.4) only occur if titanium dioxide is used as make-up chemical. Reaction (2.4) and (2.5) occur in the black liquor gasification unit at elevated temperatures. Reaction (2.6) takes place in the leaching plant, where water and sodium pentatitanate react and form sodium hydroxide and sodium trititanate.

$$Na_2CO_3\,(s) + 3TiO_2\,(s) \rightarrow Na_2O \cdot 3TiO_2\,(s) + CO_2\,(g) \qquad (2.4)$$

$$7Na_2CO_3\,(s) + 5(Na_2O \cdot 3TiO_2)\,(s) \rightarrow 3(4Na_2O \cdot 5TiO_2)\,(s) + 7CO_2\,(g) \qquad (2.5)$$

$$3(4Na_2O \cdot 5TiO_2)\,(s) + 7H_2O \rightarrow 5(Na_2O \cdot 3TiO_2)\,(s) + 14NaOH\,(aq) \qquad (2.6)$$

Other possible reactions involving titanates that might occur in the gasifier are:

$$Na_2CO_3\,(s) + 4Na_2O \cdot 5TiO_2\,(s) \rightarrow 5(Na_2O \cdot TiO_2)\,(s) + CO_2\,(g) \qquad (2.7)$$

$$Na_2CO_3\,(s) + 6TiO_2\,(s) \rightarrow Na_2O \cdot 6TiO_2\,(s) + CO_2\,(g) \qquad (2.8)$$

It is desirable to obtain sodium pentatitanate from the gasifier since it, in contact with water in the leaching plant, form sodium hydroxide, i.e. white liquor, and sodium trititanate, which can be recycled to the gasifier.

Kiiskilä (1979) showed experimentally that in the temperature range 850-950°C the equilibrium of Reaction (2.7) shifted to the left-hand side if the reaction atmosphere was changed to carbon dioxide, i.e. mainly sodium pentatitanate were formed. This was confirmed by Zou (1991) who found that sodium metatitanate, $Na_2O{\cdot}TiO_2$, is not formed as a product when heating the sample in a carbon dioxide atmosphere.

In the conventional process all energy has to be delivered at high temperatures (850-950°C) for calcination to take place. About half of the energy delivered during calcination is released at low temperature (100°C) during slaking and causticization. That is, the process has poor energy economy. In the titanate process, the main reactions, Reaction (2.4) to (2.6), are endothermic. About half of the energy needed at the high temperature in the conventional process is needed at the high temperature (850°C) for Reaction (2.5) to take place. A small amount of energy is needed at low temperatures (100°C) for Reaction (2.6) to take place. No energy delivered at high temperature is released at low temperature, which results in a better heat economy for the titanate process than for the conventional process.

A great advantage with this process is the possibility to separate the two pulping chemicals (NaOH and Na_2S). Approximately 80% of the sulphur in the black liquor form gaseous products, mainly hydrogen sulphide, H_2S (Zeng and van Heiningen, 1998). The gaseous stream from the gasifier is scrubbed giving a sulphur-containing stream and a clean flue gas, which can be used for power generation. The solid stream formed, mainly consisting of sodium pentatitanate, is hydrolysed in the leaching plant forming sodium trititanate, which is separated from the caustic solution and recycled to the gasifier. From the gaseous stream sulphide-rich white liquor is formed while the solid stream yields sulphide-lean white liquor. Depending on the application, the two white liquor streams can be mixed giving a tailor made white liquor.

Compared to the conventional process, direct causticization has several advantages:

- It is possible to increase the ratio between electricity and steam produced.
- The external energy demand is reduced substantially.
- The dead load of sodium carbonate is eliminated.
- White liquors with different sulphidity can be obtained.

One disadvantage with this process might be the price of causticizing agents. Other possible disadvantages, that need further investigation, are the possible accumulation of non-process elements and dead load of metal oxides.

3 SOLID-SOLID REACTIONS

Solid-solid reactions, also called solid state reactions or mixed powder reactions, are reactions where at least one of the reactants is solid. According to Tamhankar and Doraiswamy (1979) there are three different types of solid-solid reactions:

- Simple addition, where solid reactants react to give a solid product.
- Addition by elimination where, in addition to the solid product, a gaseous product is involved.
- Exchange, where cations and anions of the reactants are exchanged to give products.

A solid-solid reacting system can be divided into four different parts. First, two solid reactants contact each other and an initial surface reaction takes place. Then at least one of them diffuses first due to self-diffusion and thereafter through the product shell. Finally, when the diffusing reactant reaches the other reactant, reaction continues and the product shell grows thicker.

There are several possibilities for product growth:
1. Product growth controlled by diffusion of the reactants through a continuous product layer.
2. Product growth controlled by nucleation and nuclei growth.
3. Product growth controlled by reaction kinetics:
   a) Phase-boundary equations.
   b) Kinetic equations based on the concept of an n-order of reaction.

Mass transfer controls most solid-solid reactions, that is, diffusion is the rate-limiting step. Many studies of systems similar to that of sodium trititanate and sodium carbonate have shown diffusion controlled kinetics (Palm and Theliander, 1997; Zou, 1991).

3.1 Kinetic Models

Some examples of commonly used models for solid-solid reactions are shown in Table 3.1. Jander and Valensi-Carter are kinetic models controlled by product layer diffusion and the most widely used models in solid-solid reaction rate studies (Jander, 1927; Carter, 1961). These models are often called “shrinking-core models”, that is, they assume that the product surrounds a core of reactant. Assumptions made for these kind of solid-solid kinetic models are that the reactant particles are spherical and that surface diffusion rapidly covers the reactant

particles with a continuous product layer during the initial stage of the reaction. It is also assumed that further reaction takes place by bulk diffusion of a mobile reactant species through the product layer, which is the rate-controlling step. The Valensi-Carter model takes account for the change in volume due to reaction by introducing the parameter z, and is the diffusion-controlled model used in this thesis. The Jander model is a simpler model and is based on the assumption that the reacting spherical shell is a plane sheet when the diffusion equation is applied. This simplification leads to the fact that this model is only valid when the ratio of the inner and outer surface of the product shell is small. In addition, the total radius of reacted and unreacted material is assumed to be constant throughout the reaction.

Table 3.1. Models used to describe solid-solid reactions. x is the degree of conversion ($0 \le x \le 1$), k is the rate constant, t is the time, z is the volume of product formed per volume of reactant consumed, r is the radius and r_0 is the initial radius of the reactant sphere.

Model and Source	Rate-Controlling step	Equation (integrated)
Jander Jander, 1927	Diffusion	$\frac{2k}{r_0^2}t = \left(1-(1-x)^{1/3}\right)^2$
Valensi-Carter Carter, 1961	Diffusion	$\frac{2(1-z)k_1}{r_0^2}t + z = (1+(1-z)x)^{2/3} + (z-1)(1-x)^{2/3}$
Phase-boundary Tamhankar and Doraiswamy, 1979	Chemical kinetics for first-order equation	$\frac{k_2}{r_0}t = 1-(1-x)^{1/3}$
Modified shrinking-core	Diffusion and chemical kinetics	$t = -\frac{r-r_0}{k_3} - \frac{\left(\frac{r^2-r_0^2}{2} - \frac{1}{2(1-z)}\left(\left(r^3(1-z)+zr_0^3\right)^{2/3} - r_0^2\right)\right)}{k_4}$

When diffusion of the reactant species through the product layer is fast compared to the reaction rate, the reaction rate is controlled by phase-boundary reactions, i.e. chemical kinetics. In the phase boundary model it is assumed that reaction is slow compared to diffusion, but fast enough to occur in a very shallow layer near the

interface. If solid A is the diffusing species, reaction in the bulk of the other solid reactant, B, is not given any consideration.

Three different models have been used in this work, the Valensi-Carter model, the phase boundary model based on spherical geometry and a "modified shrinking-core model". The expressions for these models will be derived below.

3.1.1 The Valensi-Carter Model

The Valensi-Carter model (Carter, 1961) is a so-called shrinking-core model for spherical particles. The parameter z is introduced to describe the volume of product formed per unit volume of reactant consumed, i.e. the change in total radius.

The following reaction:

A (s) + B (s) $\rightarrow$ C (s)

can be used to explain the shrinking-core concept and to derive the Valensi-Carter expression.

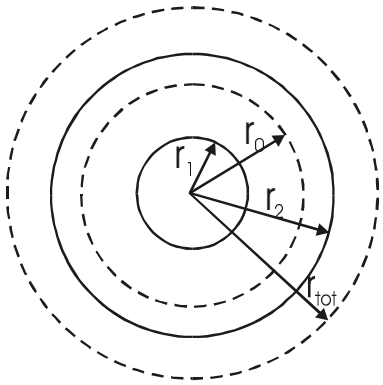

Figure 3.1. Model for the reaction of a sphere of component A with component B. r_0 = initial radius of A; r_1 = instantaneous radius of A; r_{tot} = radius of product at x=1.0; and r_2 = instantaneous radius of unreacted A plus product.

Reactants A and B and product C are solid throughout the reaction. Reactant A is a solid sphere with initial radius r_0. As the reaction proceeds a product shell of C is formed, around a core of reactant A, with inner radius r_1 and outer radius r_2 (Figure 3.1). B is the only diffusing species, and it diffuses uniformly into the product layer

around the entire sphere. r_{tot} is the final radius of product, i.e. when reaction is completed, and total conversion, x=1.0, is obtained.

The mass transfer equation for spheres is defined as:

$$\frac{\partial c}{\partial t} = \frac{1}{r^2}\frac{\partial}{\partial r}\left(D_{eff} r^2 \frac{\partial c}{\partial r} \right) + \frac{1}{r^2 \sin\theta}\frac{\partial}{\partial \theta}\left(D_{eff} \sin\theta \frac{\partial c}{\partial \theta} \right) + \frac{D_{eff}}{r^2 \sin^2\theta}\frac{\partial^2 c}{\partial \varphi^2} \qquad (3.1)$$

where D_{eff} is the effective diffusion coefficient (m^2/s), c is the concentration of the diffusing species (mol/m^3) and r is the radius of the sphere (m). If only radial diffusion is assumed ($\partial c/\partial\theta = 0 \text{ and } \partial^2 c/\partial\varphi^2 = 0$) as well as the reaction to be treated as pseudo steady-state ($\partial c/\partial t = 0$) and the diffusivity to be constant, the mass transfer equation reduces to:

$$\frac{d}{dr}\left(r^2 \frac{dc}{dr} \right) = 0 \qquad (3.2)$$

or

$$\frac{d^2 c}{dr^2} + \frac{2}{r} \cdot \frac{dc}{dr} = 0 \qquad (3.3)$$

Solving this expression with the boundary conditions $c=c_1$ at $r=r_1$ and $c=c_2$ at $r=r_2$, that is, constant concentration at the interface between the reactants and the product shell, gives the following result:

$$c = \frac{c_1 r_1 (r_2 - r) + c_2 r_2 (r - r_1)}{r(r_2 - r_1)} \qquad (3.4)$$

which in differential form is written:

$$\frac{dc}{dr} = \frac{1}{r^2} \cdot \frac{r_1 r_2 (c_2 - c_1)}{(r_2 - r_1)} \qquad (3.5)$$

Fick's first law defines the radial flow of diffusing species B as:

$$\frac{dn_B}{dt} = -D_{eff} \cdot 4\pi r^2 \cdot \frac{dc}{dr} \qquad (3.6)$$

where n_B is the amount of diffusing species B (mol). The sign of the flow rate is negative since the mass transport is in the opposite direction to the radius. Combining Equation (3.5) and (3.6) gives:

$$\frac{dn_B}{dt} = -D_{eff}\left(c_2 - c_1\right)\cdot\frac{4\pi r_1 r_2}{\left(r_2 - r_1\right)} \tag{3.7}$$

If the reaction is equimolar between A and B the quantity change of B is equal to the quantity change of A, and can be expressed:

$$dn_B = dn_A = \rho_{mA}\cdot 4\pi r_1^2\cdot dr_1 \tag{3.8}$$

where ρ_{mA} is the molar density of reactant A (mol/m³). If Equation (3.7) and (3.8) are combined, which can be done since B is the only diffusing species, the following expression is obtained:

$$\frac{dr_1}{dt} = -\frac{D_{eff}\left(c_2 - c_1\right)}{\rho_{mA}}\cdot\frac{r_2}{r_1\left(r_2 - r_1\right)} = -k_1\cdot\frac{r_2}{r_1\left(r_2 - r_1\right)} \tag{3.9}$$

where k_1 is the rate constant (m²/s), defined as:

$$k_1 = \frac{D_{eff}\left(c_2 - c_1\right)}{\rho_{mA}} \tag{3.10}$$

If reaction between A and B is not equimolar, the stoichiometric coefficients will be included in the expression for the rate constant above (Equation 3.10). To take account for the fact that the volume of the sphere is changing during reaction, the factor z is introduced. The instantaneous total radius (r_2) can therefore be written:

$$r_2 = \left(z r_0^3 + r_1^3\left(1 - z\right)\right)^{1/3} \tag{3.11}$$

If Equation (3.11) is inserted in Equation (3.9) the differential form of the Valensi-Carter expression is obtained:

$$\frac{dr_1}{dt} = -k_1\cdot\left(r_1 - \frac{r_1^2}{\left(z r_0^3 + r_1^3\left(1 - z\right)\right)^{1/3}}\right)^{-1} \tag{3.12}$$

where k_1 is the rate constant (m²/s), r_0 is the initial radius of reactant A (m) and r_1 is the instantaneous radius of reactant A (m).

If the differential form of the Valensi-Carter model is integrated from $r_0 \rightarrow r$ and $0 \rightarrow t$, and the radius, r, is substituted by the degree of conversion, x, the following expression is obtained:

$$(1+(z-1)x)^{2/3} + (z-1)(1-x)^{2/3} = z + \frac{2(1-z)k_1 t}{r_0^2} \qquad (3.13)$$

where the degree of conversion, x, is:

$$x = 1 - \left(\frac{r_1}{r_0}\right)^3 \qquad (3.14)$$

3.1.2 The Phase Boundary Model

When the mass transport of the reactant through the product layer is fast compared to the reaction, the model can be described by chemical kinetics. The phase boundary model is derived from the expression for a first-order reaction and assumes that the interface between the product layer and the core of reactant moves with a constant radial velocity. Consider the reaction:

A (s) + B (s) $\rightarrow$ C (s)

where reactants A and B and product C are solid throughout the reaction. Reactant A is a solid sphere with initial radius r_0. As the reaction proceeds a product shell of C is formed around a core of reactant A, with inner radius r_1 and outer radius r_2 (Figure 3.1). For a first order reaction, reaction rate, η is defined as:

$$\eta = \frac{dn_B}{dt} = -k_r \cdot c_1 \cdot A_1 = -k_r \cdot c_1 \cdot 4\pi r_1^2 \qquad (3.15)$$

where n_B is the amount of diffusing species B (mol), A_1 is the inner surface area (m^2), k_r is the reaction rate constant (m/s) and c_1 is the concentration of A on the inner surface of the sphere (mol/m^3).

If the reaction is equimolar between A and B the quantity of B is equal to the quantity of A, and the amount of B, n_B, can be expressed as:

$$n_B = n_A = \rho_{mA} \cdot \frac{4\pi}{3} \cdot r_1^3 \qquad (3.16)$$

where ρ_{mA} is the molar density of reactant A (mol/m³). Differentiation of Equation (3.16) gives:

$$\frac{dn_B}{dr_1} = 4\pi \cdot \rho_{mA} \cdot r_1^2 \qquad (3.17)$$

Combining Equation (3.15) and (3.17) gives the phase boundary model for first order reaction with spherical geometry:

$$\frac{dr_1}{dt} = -\frac{k_r \cdot c_1}{\rho_{mA}} = -k_2 \qquad (3.18)$$

where k_2 is the reaction rate constant (m/s). Integrating this expression from $r_0 \rightarrow r$ and $0 \rightarrow t$, and substitute the radius, r, by the degree of conversion, x, yields the integrated form of the phase boundary model:

$$k_2 t = \left(1 - (1-x)^{1/3}\right) \cdot r_0 \qquad (3.19)$$

3.1.3 The Modified Shrinking-Core Model

Both diffusion and chemical kinetics for a first-order reaction influence product growth for the modified shrinking-core model. The model assumes a sphere reacting from the surface and towards the centre. The change of total radius is taken into account by using the ratio z, as in the Valensi-Carter model.

In the Valensi-Carter model boundary conditions with constant concentration at the core is used, the modified shrinking-core model is instead derived using the following boundary condition:

$$D_{eff} \cdot \frac{dc}{dr} = k_r \cdot c \quad \text{at} \quad r = r_1 \qquad (3.20)$$

where D_{eff} is the effective diffusion coefficient (m²/s), k_r is the reaction rate constant (m/s) and c is the concentration of the diffusing species B (mol/m³). This is a mass balance meaning that the diffusing species is consumed at the interface by a first order reaction. The other boundary condition is unchanged ($c=c_2$ at $r=r_2$), meaning that the concentration at the surface of the sphere is constant. Lindman and Simonsson (1979) performed a study using this set of boundary conditions.

They derived a kinetic model for solid-liquid reactions. The two boundary conditions are valid both for solid-liquid reactions and solid-solid reactions but, in the case of one liquid reactant, c stands for the liquid reactant concentration.

The mass transfer equation for a sphere is simplified in the same way as for the Valensi-Carter model, and, solved with these new boundary conditions gives:

$$\rho_{mA} \cdot \frac{dr_1}{dt} = \frac{-c_2}{\left(\frac{1}{k_r} + \left(\frac{r_1}{r_2} - \frac{r_1^2}{r_2^2} \right) \cdot \frac{r_2}{D_{eff}} \right)} \tag{3.21}$$

which can also be written as:

$$\frac{dr_1}{dt} = \frac{-1}{\frac{1}{k_r \cdot \frac{c_2}{\rho_{mA}}} + \frac{1}{D_{eff} \cdot \frac{c_2}{\rho_{mA}}} \left(r_1 - \frac{r_1^2}{r_2} \right)} \tag{3.22}$$

From Equation (3.22), k_3 and k_4 can be identified as:

$$k_3 = k_r \cdot \frac{c_2}{\rho_{mA}} \tag{3.23}$$

$$k_4 = D_{eff} \cdot \frac{c_2}{\rho_{mA}} \tag{3.24}$$

where c_2 is constant. If the reaction between A and B is not equimolar, the stoichiometric coefficients will be included in the rate constants above, Equation (3.23) and (3.24). The outer radius of the product shell, r_2, can be expressed as for the Valensi-Carter model:

$$r_2 = \left(z r_0^3 + r_1^3 (1 - z) \right)^{1/3} \tag{3.25}$$

The differential equation of the modified shrinking-core model can finally be expressed as:

$$\frac{dr_1}{dt} = -\left(\frac{1}{k_3} + \frac{1}{k_4} \cdot \left(r_1 - \frac{r_1^2}{\left(z r_0^3 + r_1^3 (1-z) \right)^{1/3}} \right) \right)^{-1} \tag{3.26}$$

where k_3 is the reaction rate constant for the first-order reaction (m/s), k_4 is the lumped diffusivity (m²/s) and r_0 is the initial radius of the sphere (m). If the value of k_3 is very large compared to the value of k_4, the first term in Equation (3.26) becomes very small and can therefore be neglected, the model is then identical to the Valensi-Carter model. If instead the value of k_4 is much larger than the value of k_3 the second term in the modified shrinking-core model can be neglected and the model turns into a phase boundary model.

If Equation (3.26) is integrated between $r_0 \rightarrow r$ and $0 \rightarrow t$, the following expression is obtained:

$$t = -\frac{r - r_0}{k_3} - \frac{\left(\frac{r^2 - r_0^2}{2} - \frac{1}{2(1-z)} \left(\left(r^3 (1-z) + z r_0^3 \right)^{2/3} - r_0^2 \right) \right)}{k_4} \tag{3.27}$$

4 EXPERIMENTAL

4.1 Sample Preparation

The sample was prepared by dissolving sodium carbonate (Na_2CO_3) in distilled water and then adding sodium trititanate ($Na_2O{\cdot}3TiO_2$). The suspension, stirred with a magnetic stirrer, was heated to its boiling point to evaporate water. When the concentration of solids in the suspension became very high, the magnetic stirrer could not operate properly and the sample was put in a furnace (105°C) to dry overnight. Finally, the dried sample was ground to a fine powder. The powder was sieved and only the sizefraction below 210 μm was used. The molar ratio used in all the experiments was $Na_2O{\cdot}3TiO_2$/ Na_2CO_3 = 5/7, which corresponds to the stoichiometric ratio. Sodium trititanate of 99% purity was obtained from Aldrich Chemical Company, Inc., and sodium carbonate, pro analysis, from Merck.

4.2 The Equipment

The reaction was carried out in a differential reactor made of quartz glass enclosed in a furnace, Figure 4.1. The quartz glass reactor consists of three concentric pipes. The sample was placed in a sample holder on top of the innermost pipe. The gas was heated as it flowed upwards in the reactor between the two outer pipes. At the top of the reactor the gas was forced down the inner pipe and through the sample, which was resting on a porous bed of quartz glass inside the sample holder. The sample was placed in the furnace by removing the innermost pipe, placing the sample holder on top of it and then replacing it in the furnace. A detailed description of the equipment and procedure can be found elsewhere (Hanson, 1993).

The concentration of carbon dioxide in the reject gases (vol-%) was measured by a NDIR (non-dispersive infrared) industrial photometer (URAS 3G, Mannesmann, Hartman & Braun). The signals from the measurements of temperature, carbon dioxide concentration in the outlet gas and the mass flow of the inlet gas were recorded continuously every 4 seconds by a data acquisition unit.

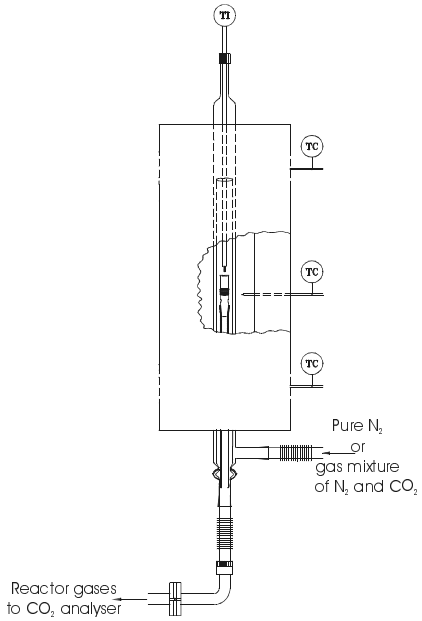

Figure 4.1. The quartz glass reactor.

The temperature in the reactor was measured by a thermocouple (Chromel-Alumel), with an accuracy of about ±10°C.

The mass flow of gas was determined by a mass flow controller (Brooks, model 5851E) run by Brooks control and read out equipment.

4.3 Procedure

The gas flow and furnace temperature were allowed to stabilise one hour before the beginning of an experimental session. In each run, 0.70 g of sample was placed in the sample holder, which was shaken gently before it was placed in the reactor to obtain a similar porosity and horizontal surface for all sample beds. The amount of sample was chosen based on the limitations of the equipment and to obtain accurate and reproducible results for the specific surface area measurements. The amount of sample was not allowed to vary more than ± 0.0009 g.

When the system became stable the gas flow was interrupted and the sample holder was placed into the reactor as quickly as possible. The gas flow was then turned on again and increased to about 10 l_{STP}/min. It took approximately 45 s from the moment when the gas flow was turned off until it was turned on again.

When the reaction was completed, i.e. the carbon dioxide content in the reject gas stabilised at the same level as before the sample was inserted, the gas flow was turned off and the sample holder removed from the reactor. The sample was cooled with nitrogen and weighed while still in the sample holder. The sample was then transferred to a sample tube for specific surface area measurements.

The specific surface area of the product was measured by a five-point nitrogen adsorption method using a Micrometrics Gemini 2370. Using the theory of Braunauer, Emmet and Teller, the surface area was calculated from the measurements of the adsorbed amount of nitrogen at five different pressures, i.e. a five point BET surface area was calculated.

The reaction was studied at five different temperatures: 800°C, 820°C, 840°C, 860°C and 880°C, and with five different amounts of carbon dioxide in the inlet gas: 0 %, 0.5 %, 1 %, 2 % and 5 %. Table 4.1 shows the number of experiments at each set of conditions.

Table 4.1. The number of experiments for each set of conditions.

	800°C	820°C	840°C	860°C	880°C
0 %	7	6	4	3	3
0.5 %			2	3	3
1 %				3	3
2 %			1	6	3
5 %			2	4	3

Before every measurement with carbon dioxide in the inlet gas the exact concentration of carbon dioxide was measured, these values are shown in Appendix A.

5 RESULTS AND DISCUSSION

5.1 Material Characterization and Product Composition

The BET surface area for the sodium trititanate material is 1.31 g/m² and the density is 3036 kg/m³. With this information, together with the assumption that the particles are spherical, the radius of the grains can be estimated to 0.75 μm. This is used as the initial particle radius in the calculations.

Several factors might influence the sintering of the particles in this case, such as reaction temperature, reaction time, carbon dioxide concentration in the reaction atmosphere and product composition. The results of the BET surface area measurements are shown in Figure 5.1 as a function of reaction temperature and in Figure 5.2 as a function of reaction time. The BET surface area is measured for all samples. Mean values and deviations from the mean value are calculated for each set of experimental conditions. These results are presented in Table A.2 (Appendix A). The BET surface areas from this study without carbon dioxide in the inlet gas can be compared to the BET surface areas obtained from a study performed in the same equipment by Nohlgren (1999). In Nohlgren's study, the sintering increased with increasing temperature although decreasing reaction times. Thus, the temperature seemed to have a larger influence on the sintering than the reaction time. However, only a weak increase in sintering was seen for the temperatures between 800°C and 860°C. The tendency seen in this study was somewhat different; for the temperatures between 800°C to 860°C the BET surface area is almost constant, while a higher value of the BET surface area is obtained at 880°C. The reaction time is decreasing when the temperature is increasing. When comparing these results it should be kept in mind that the deviations from the mean value for some sets of conditions are significant. However, it is clear that Nohlgren's study show less sintered samples than found in this study, except for the sample at 880°C, which is more sintered.

The experiments with carbon dioxide in the inlet gas show higher BET surface areas than the experiments without carbon dioxide, i.e. the sample sinter less when the reaction occur in a carbon dioxide atmosphere. However, no clear connection between the amount of carbon dioxide and the sintering can be seen; the experiments with 0.5% and 5% CO_2 show lower BET surfaces than experiments with 1% and 2% CO_2. The highest BET surface is found for the experiments with 2% CO_2 in the inlet gas at 860°C. When the temperature is decreased from 880°C to 860°C experiments with 0.5% CO_2 show increased sintering, experiments with 1% and 2% CO_2 show decreased sintering and experiments with 5% CO_2 show almost constant BET surface areas. Though, when the temperature is further

decreased to 840°C, for 0.5%, 2% and 5% CO_2, and the reaction time is increased as well, the sintering is increasing.

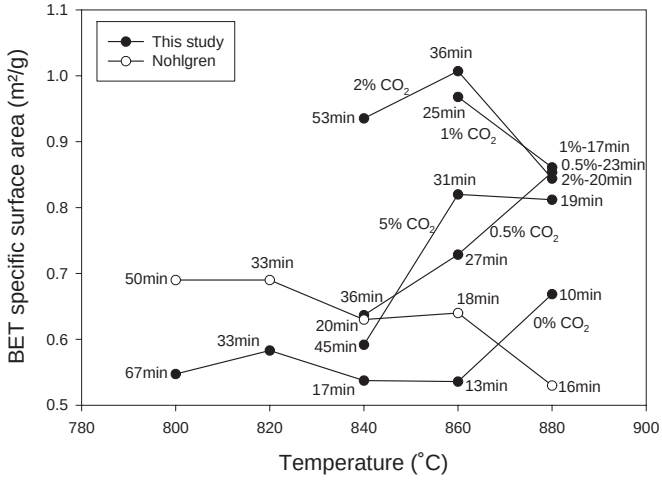

Figure 5.1. Mean values of the BET specific surface area versus reaction temperature.

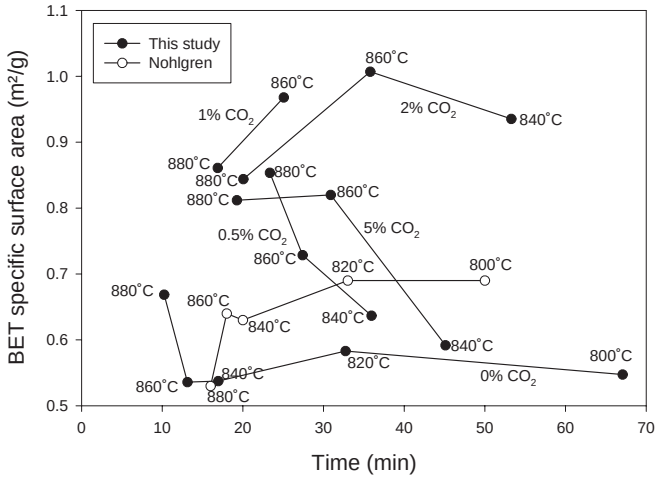

Figure 5.2. Mean values of the BET specific surface area versus reaction time.

Also in this case it should be kept in mind that the deviations from the mean values are significant. However, one interesting point is that at 880°C the experiments with carbon dioxide have almost similar reaction times and the BET surface area seem to be independent to the CO_2 concentration. As mentioned earlier several factors might influence the sintering of the particles. This might explain the fact that no clear pattern can be seen in Figure 5.1 and 5.2 since reaction time and temperature, carbon dioxide concentration and product composition respectively are dependent of each other in this study.

The product composition was investigated by X-ray diffraction (XRD) analysis. It should be pointed out that the XRD analysis cannot be regarded as being quantitative, but the dominating compounds can be identified. XRD analysis have been performed for experiments with 0%, 0.5% and 5% CO_2 in the inlet gas and at the temperatures 840, 860 and 880°C. Without carbon dioxide in the inlet gas the products from the experiments at all temperatures contained unreacted sodium trititanate, $Na_2O{\cdot}3TiO_2$, and the products sodium pentatitanate, $4Na_2O{\cdot}5TiO_2$, and sodium metatitanate, $Na_2O{\cdot}TiO_2$. For the experiments at all temperatures with 0.5% and 5% CO_2 in the inlet gas, only unreacted sodium trititanate and the product sodium pentatitanate was found. Consequently, no metatitanate was found in the samples from the experiments carried out in a carbon dioxide atmosphere. This is consistent with Zou's (1991) results, i.e. that reaction (2.7) is shifted to the left in a carbon dioxide atmosphere.

The different product composition for experiments with and without carbon dioxide might explain why the experiments carried out in a carbon dioxide atmosphere show less sintering than experiments without carbon dioxide. Table 5.1 shows the crystal structures, crystal densities and melting points for different sodium titanates. Sodium metatitanate occurs in three different crystal structures, the one that is found in the products from this study is the β-structure. Sodium pentatitanate, which is triclinic and sodium trititanate, which is monoclinic, have higher crystal densities than β-sodium metatitanate, which is monoclinic.

Table 5.1. Crystal structures, crystal densities and melting points for different sodium titanates.

Titanate	Crystal structure	$\rho_{crystal}$ (g/cm³)	Melting point[4)] (°C)
α-$Na_2O{\cdot}TiO_2$	Face-centred cubic[1)]	3.47 [1)]	965
β-$Na_2O{\cdot}TiO_2$	Monoclinic[1)]	3.29 [1)]	965
γ-$Na_2O{\cdot}TiO_2$	Monoclinic[1)]	2.93 [1)]	965
$Na_2O{\cdot}3TiO_2$	Monoclinic[2)]	3.43 [2)]	1130
$4Na_2O{\cdot}5TiO_2$	Triclinic[3)]	3.32 [3)]	1030

[1)] Index to the Powder Diffraction File
[2)] Andersson and Wadlsey (1961)
[3)] Takei (1976)
[4)] Zou (1991)

It can also be seen that sodium metatitanate has the lowest melting point, which might indicate that it will sinter easier than sodium pentatitanate and sodium trititanate. Consequently this gives a lower BET surface area for the experiments without carbon dioxide, which contains sodium metatitanate. Another possible explanation could be that when sodium pentatitanate is formed, only one structural change occurs; from monoclinic to triclinic. When sodium metatitanate is formed instead, there is an extra structural change. First, triclinic sodium pentatitanate is formed and thereafter monoclinic sodium metatitanate, which might result in a lower BET surface area.

5.2 Kinetic Results

The carbon dioxide concentration in the outlet gas and the temperature in the reaction zone were measured continuously during the experiments. Figure 5.3 shows examples of the CO_2-concentration and the temperature profiles versus time at 880°C and (a) 0% CO_2 and (b) 2% CO_2 in the inlet gas.

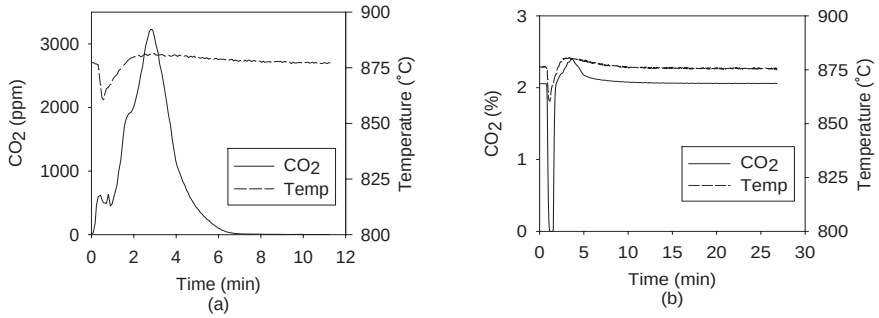

Figure 5.3. Carbon dioxide concentration and temperature versus time for experiments at 880°C and (a) 0% CO_2 and (b) 2% CO_2 in the inlet gas.

For the experiments without carbon dioxide in the inlet gas, the concentration of carbon dioxide in the outlet gas increases when the gas flow is interrupted and the sample holder is removed. This is probably due to the fact that air is sucked into the system and the graphs therefore show a peak or plateau at approximately 500 ppm CO_2, i.e. the concentration in air. The temperature starts to decrease when the sample holder is removed and the lowest temperature is obtained when the cold sample holder with sample is replaced into the reactor, since much cold mass is introduced to the system. From the time when the sample holder is replaced to the time when the gas flow is turned on again, approximately 15-20 seconds, carbon

dioxide is produced by the reaction and accumulated in the system. Therefore, a second CO_2-peak is obtained when the gas flow is turned on again and the accumulated amount of carbon dioxide is transported to the analyzer. The temperature starts to increase after the sample holder has been replaced and the gas flow is turned on. Approximately 70-80 seconds after the sample holder has been replaced the temperature reaches a maximum and is then stabilized at the chosen temperature. When the temperature reaches its maximum, a peak or plateaux can be seen in the carbon dioxide concentration profile.

When there is carbon dioxide in the inlet gas, the graphs of carbon dioxide concentration versus time look different, while the temperature profile looks similar to experiments without carbon dioxide. The concentration of carbon dioxide in the inlet gas is much higher than in air, and therefore the concentration decreases when the gas flow is turned off and the sample holder is removed. When the sample holder is replaced and the gas flow is turned on the carbon dioxide concentration starts to increase. The higher concentration of carbon dioxide in the inlet gas, the longer time does it take to reach the start concentration again after insertion of the sample. Thereafter there is a peak or plateaux of carbon dioxide before it starts to decrease to the same concentration as in the inlet gas. The small peaks or plateaux, due to the sucking of air into the system and the accumulation of carbon dioxide during insertion of sample, seen for experiments without carbon dioxide in the inlet gas, is not seen here. Since, these peaks are so small in relation to the concentration of carbon dioxide in the inlet gas. It takes longer time for the reaction to reach complete conversion if there is carbon dioxide in the inlet gas. This could possibly be explained by the fact that the equilibrium of Reaction (2.5) is obtained and the reaction is shifted to the left.

The conversion of sodium carbonate is calculated and plotted versus time for each experiment. For every mol of sodium carbonate consumed, one mol of carbon dioxide is produced (Reaction 2.5), therefore the measured concentration of carbon dioxide in the outlet gas can be used to calculate the degree of conversion. It is assumed that complete conversion of sodium carbonate is obtained when the carbon dioxide concentration is back at the base level after the reaction. The accumulated carbon dioxide content is then calculated, and by dividing the accumulated amount for each time by the total amount of carbon dioxide produced, the degree of conversion for each point in time can be calculated.

For the experiments without carbon dioxide in the inlet gas the starting point for the reaction in the conversion calculation is set to the time where the gas flow is turned on after the insertion of sample. For the experiments with carbon dioxide in the inlet gas the choice of starting point is more complicated. A mean value of the last approximately 30 measured values of carbon dioxide concentration is calculated and is thereafter subtracted from all the values of carbon dioxide concentration in the experiment. Negative values obtained are set to zero. The

starting points for the conversion calculation for each experiment is set to the point were the carbon dioxide concentration starts to increase above 0% after the time when the gas flow is turned on after the insertion of sample.

When more than one measurement was made for a set of experimental conditions, an average conversion degree was calculated (Figure 5.4 and 5.5). The deviation between the conversion for each experiment and the average conversion is calculated as follows:

$$\text{Deviation} = \frac{\sum_{i=1}^{n} \left| \frac{x_{av,i} - x_{exp,i}}{x_{av,i}} \right|}{n} \qquad (5.1)$$

where $x_{av,i}$ is the average degree of conversion at time i, $x_{exp,i}$ is the experimental degree of conversion at time i and n is the number of time points for which the calculation is made. The mean deviation for all experiments is calculated to be 5.5%.

Figure 5.4 shows the conversions for different temperatures at 0% and 2% CO_2 in the inlet gas. It can be seen that when the temperature is increased the reaction reach complete conversion faster, which can be seen for the other carbon dioxide levels (0.5%, 1% and 5%) as well.

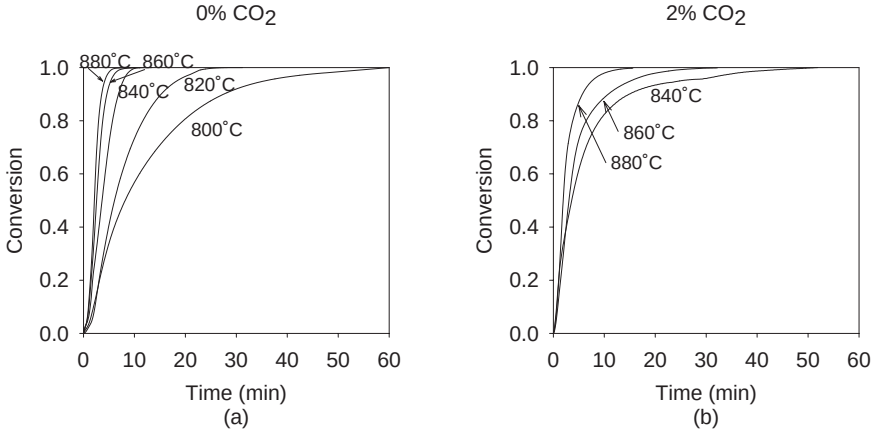

Figure 5.4. The average conversion degree of Na_2CO_3 versus time for experiments carried out at different temperatures for (a) 0% CO_2 and (b) 2% CO_2 in the inlet gas.

Figure 5.5 shows the average conversion degree at constant temperature with varying carbon dioxide concentration. It can be seen for all temperatures that the

experiments without carbon dioxide in the inlet gas reach complete conversion first. Differences can be seen between experiments with and without carbon dioxide, but no clear differences are seen between experiments with different concentrations of carbon dioxide in the inlet gas.

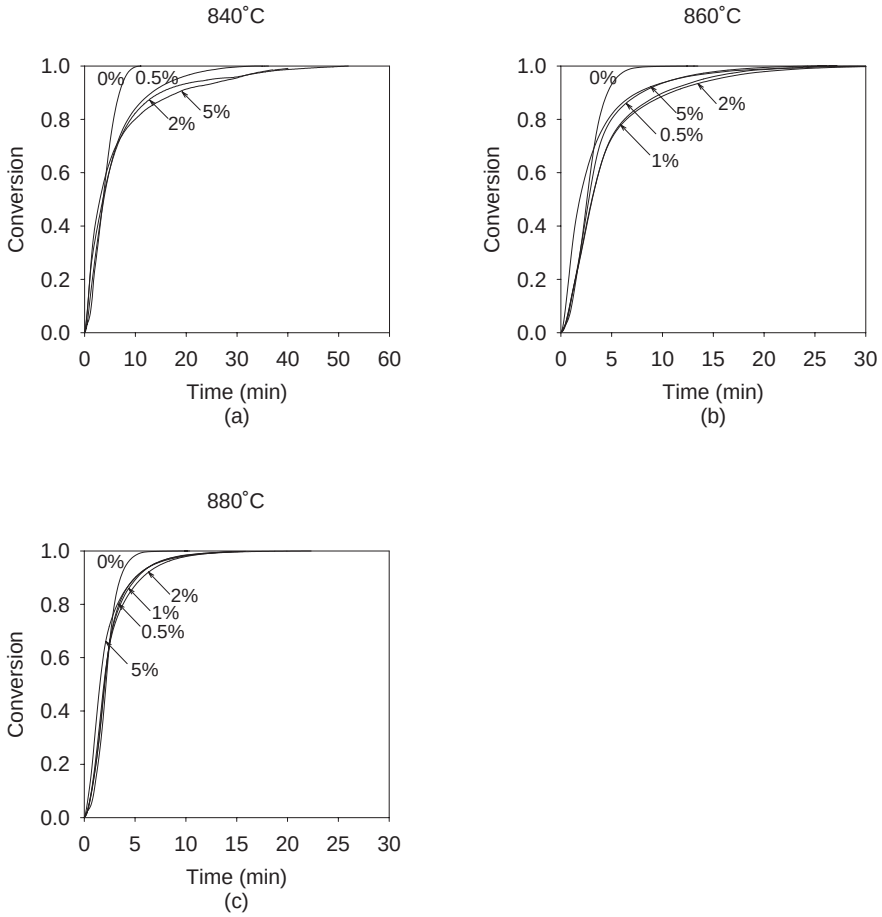

Figure 5.5. The average conversion degree of Na_2CO_3 versus time for different concentrations of carbon dioxide at (a) 840°C, (b) 860°C and (c) 880°C.

One source of possible error in the results is that the experiment was terminated manually when complete conversion was expected, i.e. when the carbon dioxide concentration in the outlet gas had stabilized. However, the carbon dioxide concentration showed small fluctuations in the end of the reaction. It was, therefore, difficult to decide when the reaction had reached complete conversion. This can explain some of the variations between different experiments at the same set of experimental conditions. Especially at 860°C and with 1% CO_2 in the inlet

gas the results were confusing in relation to the other experiments. Therefore, complementary measurements were made. It then turned out that the new measurements had to be carried out approximately twice as long time as the old ones. This indicate that the first measurements at this set of conditions were not given enough time to reach complete conversion. Therefore, only the new results are used when the average degree of conversion is calculated.

5.3 Fitting of the Kinetic Models to Experimental Data

Three different kinetic models have been used in this work:

- The Valensi-Carter model, which is controlled by diffusion.
- The phase boundary model, which is controlled by chemical kinetics for a first order reaction.
- The modified shrinking-core model, which is controlled by both diffusion and chemical kinetics.

Earlier studies of direct causticization with titanium salts have shown diffusion-controlled kinetics. Palm & Theliander (1997) used the Valensi-Carter model and the phase boundary model and Zou (1991) used the Jander model. Nohlgren (1999) used the same models as in this study, and found that a change in reaction mechanism from diffusion to chemical kinetics occurred between 840°C and 860°C for experiments made in a nitrogen atmosphere.

The fitting of the models to the experimental data is done in a conversion range from 8% to 98%, due to initial temperature fluctuations and the decreasing reaction rate at the end of the process. Since the conversion data show a clear change in the slope around a conversion degree of 73% for experiments with carbon dioxide in the inlet gas, the phase boundary model is also fitted to the experimental data in the conversion range from 8% to 73%.

The rate constants in the kinetic models were determined by fitting the model to experimental data, which was done by minimising the square sum error, using the routine “lsqnonlin” in Matlab. The reaction was then simulated, also in Matlab, solving the model differential equation using the routine “ode23”. Numerical values of the rate constants are shown in Appendix B.

The standard deviation between the fitted models and the experimental data is calculated for degrees of conversion from 8% to 98%. The standard deviation is calculated as the squared difference in degree of conversion between the experimental values and the calculated values for each point in time. The sum of the squared difference is divided by the number of points minus one for which the calculation is made. Extracting the root of this gives the standard deviation.

$$\text{Std.dev.} = \sqrt{\frac{\sum_{i=1}^{n}\left(x_{exp,i} - x_{calc,i}\right)^2}{n-1}} \qquad (5.2)$$

where $x_{exp,i}$ is the degree of conversion for the experimental values at time i, $x_{calc,i}$ is the degree of conversion for the fitted model at time i and n is the number of time points for which the calculation is made. Since several experiments are performed at each set of conditions and the models are fitted to each experiment, the mean standard deviation is calculated for each set of conditions, which is presented in Table 5.2.

Table 5.2. The mean standard deviation between degrees of conversion from 8% to 98% for the different set of conditions.

	Valensi-Carter	Phase boundary	Modified shrinking-core	Phase boundary 8-73%
0% CO_2				
800°C	0.028	0.038	0.017	
820°C	0.064	0.013	0.011	
840°C	0.105	0.026	0.032	
860°C	0.116	0.037	0.031	
880°C	0.134	0.051	0.044	
0.5% CO_2				
840°C	0.033	0.043	0.033	0.010
860°C	0.052	0.042	0.042	0.030
880°C	0.058	0.039	0.038	0.039
1% CO_2				
860°C	0.041	0.046	0.041	0.011
880°C	0.059	0.037	0.037	0.042
2% CO_2				
840°C	0.057	0.066	0.057	0.031
860°C	0.047	0.051	0.048	0.016
880°C	0.043	0.042	0.043	0.023
5% CO_2				
840°C	0.044	0.075	0.045	0.044
860°C	0.054	0.070	0.054	0.024
880°C	0.041	0.045	0.041	0.024

To investigate the Arrhenius parameters, Arrhenius plots for the rate constants are made. The Arrhenius equation is:

$$k = A \cdot e^{-E/RT} \tag{5.3}$$

which can also be written:

$$\ln(k) = \ln(A) - \frac{E}{RT} \tag{5.4}$$

where E is the activation energy (J/mol), A is the pre-exponential factor (m^2/s or m/s), k is the reaction rate constant (m^2/s or m/s), T is the temperature (K) and R is the gas constant (8.3145 J/mol,K). The Arrhenius plots show ln(k) as a function of 1/T. Linear regression yields the activation energy from the slope of the fitted line and the pre-exponential factor from the intercept with the y-axis.

5.3.1 Experiments without Carbon Dioxide in the Inlet Gas

Figure 5.6(a) shows experimental data and fitted models for an experiment at 800°C with 0% CO_2 in the inlet gas. It can be seen that the modified shrinking-core model gives the best fit to the experimental data at this set of conditions. As seen in Figure 5.6(b), i.e. at 880°C and with 0% CO_2, the experimental values show a weak S-shape, which is difficult to describe by the models. Though, the phase boundary model and the modified shrinking-core model seem to give better fit to the experimental data than the Valensi-Carter model at this set of conditions. The weak S-shape is most obviously seen for experiments at high temperatures (860°C and 880°C).

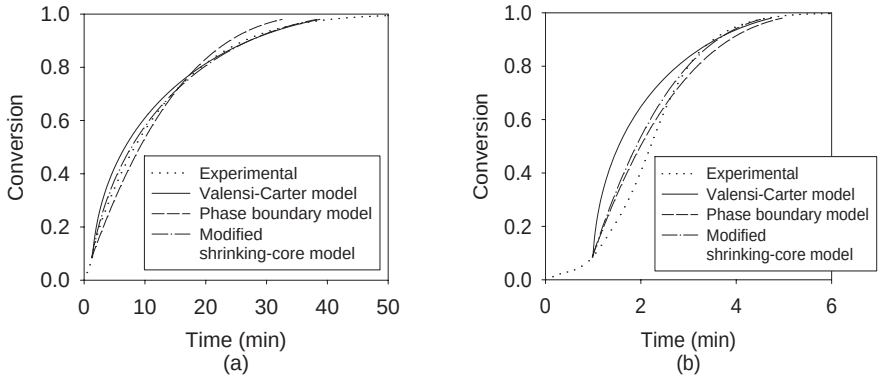

Figure 5.6. Degree of conversion versus time for the models and the experimental data for experiments with 0% CO_2 in the inlet gas at (a) 800°C and (b) 880°C.

The experiments without carbon dioxide made in this study have been compared with the results from a study made by Nohlgren (1999) in the same equipment. Figure 5.7 compares the Arrhenius plots for the two studies. The largest differences occur at 800°C for the Valensi-Carter constant, k_1, and the phase boundary constant, k_2. If these points are omitted in the linear regression, similar slopes, i.e. activation energies, are obtained for the two studies. The Arrhenius parameters are shown in Table 5.3. For the reaction rate constant, k_3, in the modified shrinking-core model there are larger differences between the two studies, especially at 800 and 820°C, and the calculated activation energies differ much. The Arrhenius plot for the diffusion constant, k_4, in the modified shrinking-core model, Figure 5.7(d), only show values at 800-820°C from this study and at 800-840°C for Nohlgren's study. This is due to the fact that at the higher temperatures k_4 is very large and the diffusion part do not affect the model. In Nohlgren's study the diffusion controlled part is significant at three temperatures (800, 820 and 840°C), so linear regression can be made. Though, in this study, the diffusion part is only significant at two temperatures (800 and 820°C), therefore there are not enough measurements to obtain a linear regression, and consequently no Arrhenius parameters are calculated. Note that the variation is larger for the diffusion constant, k_4, in the modified shrinking-core model than for the other constants in Figure 5.7.

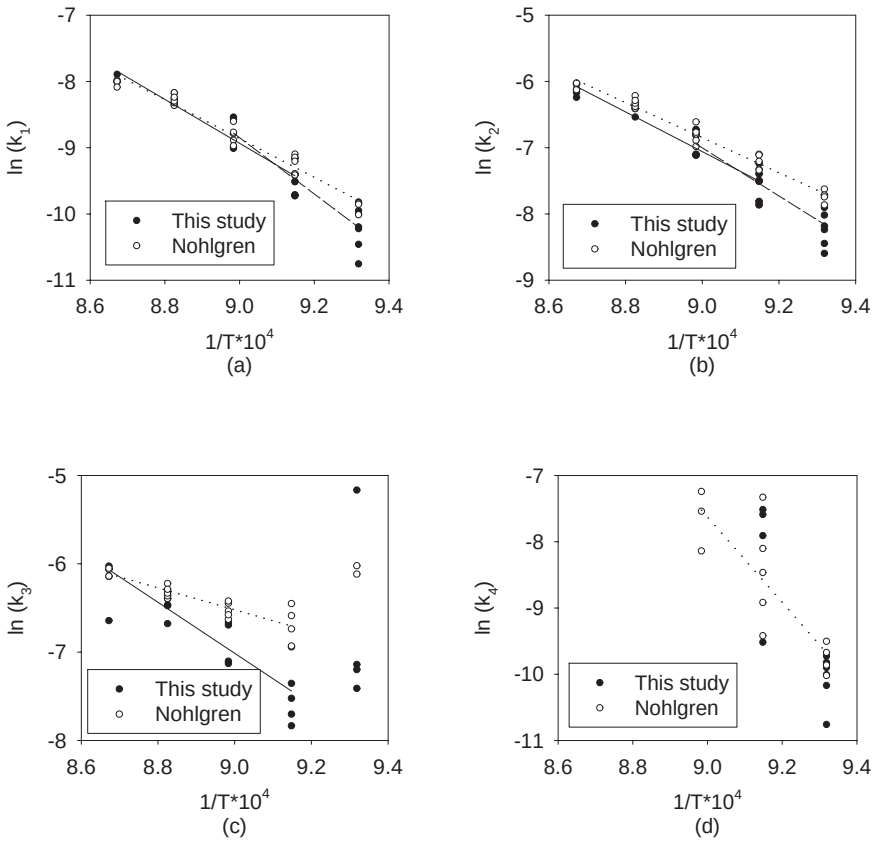

Figure 5.7. Arrhenius plots for experiments from this study with 0% CO_2 in the inlet gas and for the study made by Nohlgren (1999). (a) The Valensi-Carter constant k_1 ($\mu m^2/s$), (b) the phase boundary constant k_2 ($\mu m/s$), (c) the reaction rate constant k_3 ($\mu m/s$) and (d) the diffusion constant k_4 ($\mu m^2/s$) for the modified shrinking-core model.

Figure 5.7(a) and (b) indicate that two straight lines are needed to describe the data from this study well. One between 800°C and 840°C and one between 820°C and 880°C. This indicate a change in reaction mechanism around 820°C. In Figure 5.7(c), the pattern is not as obvious, but something seems to happen around 820-840°C.

Table 5.3. Arrhenius parameters at 0% CO_2 in the inlet gas from this study compared with the Arrhenius parameters from the study made by Nohlgren (1999).

	Pre-exponential factor, A	Activation energy, E (kJ/mol)	Temperature range
This study			
Valensi-Carter	$1.19 \cdot 10^{-3}$ m²/s	276	820-880°C
Phase boundary	444 m/s	249	820-880°C
Modified shrinking-core			
Reaction rate constant	168 m/s	240	820-880°C
Diffusion constant	-	-	
Nohlgren (1999)			
Valensi-Carter	$3.15 \cdot 10^{-5}$ m²/s	241	
Phase boundary	23.1 m/s	220	
Modified shrinking-core			
Reaction rate constant	$9.32 \cdot 10^{-5}$ m/s	102	820-880°C
Diffusion constant	$1.65 \cdot 10^{9}$ m²/s	522	800-840°C

Another way to see when the change of reaction rate controlling mechanism occurs is to compare the size of the two constants in the modified shrinking-core model, k_3 and k_4. This is easily done in Appendix B. If the reaction-rate constant, k_3, is much larger than the diffusion constant, k_4, the term in the modified shrinking-core model including k_3 can be neglected, whereas the model turns into a Valensi-Carter model, i.e. is controlled by diffusion. If instead k_4 is much larger than k_3, the model turns into a phase boundary model and the reaction is controlled by chemical kinetics. When the two constants are approximately equal, both diffusion and chemical kinetics control the reaction rate. At 800°C, in this study, k_3 is at least 10 times larger than k_4, indicating that the reaction is controlled by diffusion mechanism. At 820°C though, different experiments indicate different rate-controlling mechanisms. For three experiments k_3 and k_4 are almost equal, for one experiment is k_3 much larger than k_4 while k_4 is much larger than k_3 for two experiments. At higher temperatures, 840-880°C, k_4 is much larger than k_3, and the reaction is consequently controlled by chemical kinetics.

Figure 5.6 is an example of how the different models and the experimental data can be compared visually. Such graphs are made for every experiment. By visual judgement of these and by comparing the standard deviations between models and experimental data in Table 5.2 some conclusions can be drawn. Figure 5.6(a) shows that the modified shrinking-core model gives the best fit to the experimental data at 800°C, it also has the lowest standard deviation according to Table 5.3. At 820-880°C the lowest standard deviation between models and experimental data are obtained with the phase boundary model and the modified shrinking-core

model, and the same conclusions can be drawn by studying graphs similar to Figure 5.6.

Altogether, these results indicate a change of reaction mechanism around 820°C, with diffusion controlled kinetics below 820°C, chemical reaction controlled kinetics above 820°C and both diffusion and chemical reaction controlled kinetics at 820°C. According to Nohlgren the change in reaction mechanism occurred between 840°C and 860°C, i.e. at higher temperatures than indicating in this study. An explanation to this difference might be that the reaction times between the two studies differ much at 800°C and 820°C, but not at higher temperatures. One reason for different reaction times can be that the samples used did not have the same particle radius, though, the difference was not very large. It might also be a sign of the operator dependence of the equipment.

5.3.2 Experiments with Carbon Dioxide in the Inlet Gas

Experiments with 0.5%, 2% and 5% CO_2 in the inlet gas were carried out at 840°C, 860°C and 880°C and with 1% CO_2 in the inlet gas at 860°C and 880°C. Figure 5.8 shows the degree of conversion for the different models and the experimental data at 860°C for 0.5% and 2% CO_2 in the inlet gas. It can be seen that none of the models can describe the experimental data well in the whole interval because of the pronounced change of slope in the experimental data occurring at a conversion of approximately 70-80%, which was seen for all experiments with carbon dioxide in the inlet gas. However, the phase boundary model describes the experimental data very well for the first part of the reaction, up to a conversion of approximately 73% for almost all experiments with carbon dioxide. Note in Table 5.2 that at higher amounts of carbon dioxide in the inlet gas, not even the model that gives the best fit to the experimental data in the whole conversion interval show as low standard deviation as for experiments without carbon dioxide.

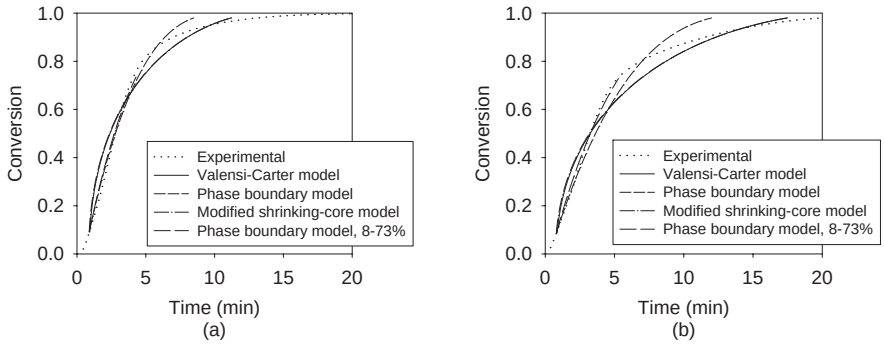

Figure 5.8. Degree of conversion versus time for the models and the experimental data for experiments at 860°C with (a) 0.5% CO_2 and (b) 2% CO_2 in the inlet gas.

Figure 5.8 is an example of how different models and the experimental data can be compared visually. Such graphs are made for every experiment. By visual judgement of these and by comparing the standard deviations between models and experimental data in Table 5.2, an indication on which mechanism that control the reaction and consequently where the change of mechanism occur can be obtained. It should be noted that the phase boundary model in the conversion interval 8-73% for many sets of conditions gives very good fit to the experimental data. This indicate that the reaction is controlled by chemical kinetics in the beginning of the reaction, which led to the idea that the reaction might be reaction controlled in the beginning and, then when the product shell have grown thicker, diffusion controlled. However, if the conversion interval between 73-98% were modelled separately, all the studied models gave very good fits. As a consequence, a two step mechanism where the reaction is controlled by chemical kinetics first and by diffusion secondly could not be shown.

Another way to see where the change of reaction mechanism occurs is to see how the reaction rate constant, k_3, and the diffusion constant, k_4, in the modified shrinking-core model are related to each other. This can easily be seen in the Arrhenius plots (Figure 5.9-5.11) or in Appendix B. If k_3 is much larger than k_4 the reaction is controlled by diffusion mechanisms and if k_4 is much larger than k_3 the reaction is controlled by chemical kinetics.

For the experiments with 0.5% CO_2 in the inlet gas (Figure 5.9) k_3 is much larger than k_4 at 840°C, which indicate that the reaction is controlled by diffusion. At 860°C and 880°C, k_4 is much larger than k_3, i.e. chemical kinetics is the rate-controlling step. According to Table 5.2 and by visual judgement of plots similar to Figure 5.8, the Valensi-Carter model and the modified shrinking-core model show the best fit to the experimental data at 840°C, while the phase boundary model and

the modified shrinking-core model describe the experimental data best at 860°C and 880°C if the models are fitted in the whole conversion interval from 8% to 98%. Linear regression for the Valensi-Carter constants, k_1, and the phase boundary constants, k_2, show that the constants can be explained by one straight line each. The phase boundary model gave very good fits to experimental data in the conversion interval 8-73% for 840°C and 860°C. For 880°C though, the experimental data showed a weak S-shape, as in Figure 5.6(b). The phase boundary model still gave good fit in the conversion range 8-73% but not as good as for the lower temperatures.

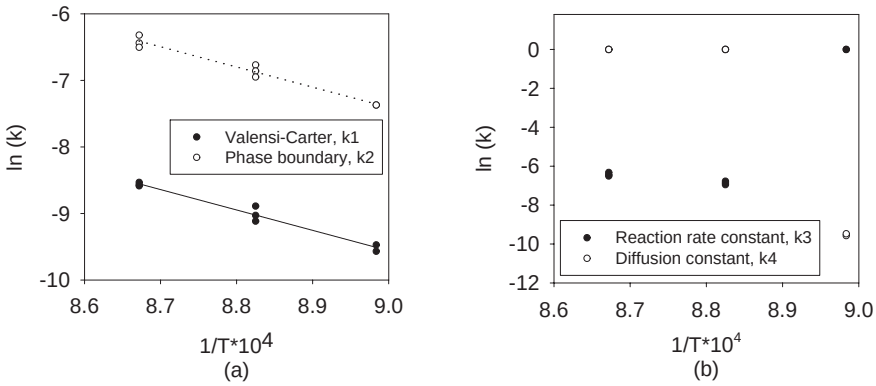

Figure 5.9. Arrhenius plots for experiments with 0.5% CO_2 in the inlet gas based on (a) the Valensi-Carter constant, k_1 ($\mu m^2/s$), and the phase boundary constant, k_2 ($\mu m/s$) and (b) the reaction rate constant, k_3 ($\mu m/s$), and the diffusion constant, k_4 ($\mu m^2/s$), for the modified shrinking-core model.

Experiments with 1% CO_2 in the inlet gas are made only at two temperatures (860°C and 880°C) and consequently no Arrhenius parameters can be calculated. Even though no Arrhenius plots are made for these experiments, the relation between k_3 and k_4 can give an indication on which mechanism that controls the reaction. At 860°C, k_3 is much larger than k_4, i.e. diffusion might be controlling the reaction rate. At 880°C though, k_4 is much larger than k_3, which indicate that chemical kinetics is the rate-controlling mechanism. Table 5.2 and visual judgement of conversion plots similar to Figure 5.8 show that the Valensi-Carter model and the modified shrinking-core model gives the best fit to the experimental data at 860°C while the phase boundary model and the modified shrinking-core model give the best fit at 880°C if the models are fitted to experimental data in the whole conversion interval. As for the experiments with 0.5% CO_2 the phase boundary model describe the experimental data very well in the conversion interval 8-73%, except at 880°C where a weak S-shape was seen.

For experiments with 2% CO_2 in the inlet gas (Figure 5.10), k_3 is much larger than k_4 for all temperatures in the interval (840-880°C) indicating that the reaction is controlled by diffusion mechanisms. When linear regression is made to calculate the Arrhenius parameters for the Valensi-Carter constants, k_1, and the phase boundary constants, k_2, it can be seen that the both straight lines describe the constants well in the interval 840-880°C. This might indicate that no change in reaction mechanism occurs in this temperature interval. Table 5.2 shows that the three models give approximately the same standard deviation from the experimental data. However, conversion plots for every experiment show that no model can describe the experimental data very well in the whole interval, but the Valensi-Carter model and the modified shrinking-core model seem to be better than the phase boundary model. Before the change of slope in the conversion curve occurring around a conversion of 73%, the phase boundary model fits the experimental data very well.

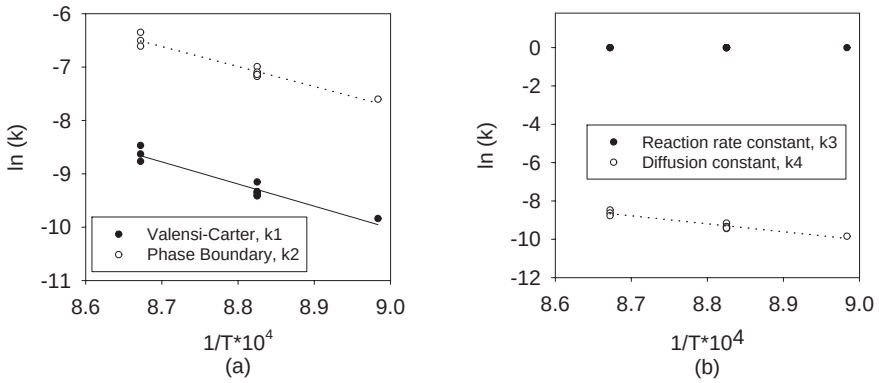

Figure 5.10. Arrhenius plots for experiments with 2% CO_2 in the inlet gas based on (a) the Valensi-Carter constant, k_1 ($\mu m^2/s$), and the phase boundary constant, k_2 ($\mu m/s$) and (b) the reaction rate constant, k_3 ($\mu m/s$), and the diffusion constant, k_4 ($\mu m^2/s$), for the modified shrinking-core model.

For experiments with 5% CO_2 in the inlet gas (Figure 5.11), k_3 is much larger than k_4 at all temperatures (840-880°C), i.e. the reaction seem to be controlled by diffusion mechanisms. None of the Valensi-Carter constants, k_1, and the phase boundary constants, k_2, show any deviation from the straight line after the linear regression is made, which indicate that no change in reaction mechanism occur in this temperature range (840-880°C). Table 5.2 shows that the Valensi-Carter model and the modified shrinking-core model give better fit to the experimental data than the phase boundary model. This is also seen in the conversion plots for each experiment, although no model seem to describe the experimental data very well in

the whole interval. However, the phase boundary model describes the experimental data very well in the conversion interval 8-73%, which was seen both visually and by the standard deviations in Table 5.2.

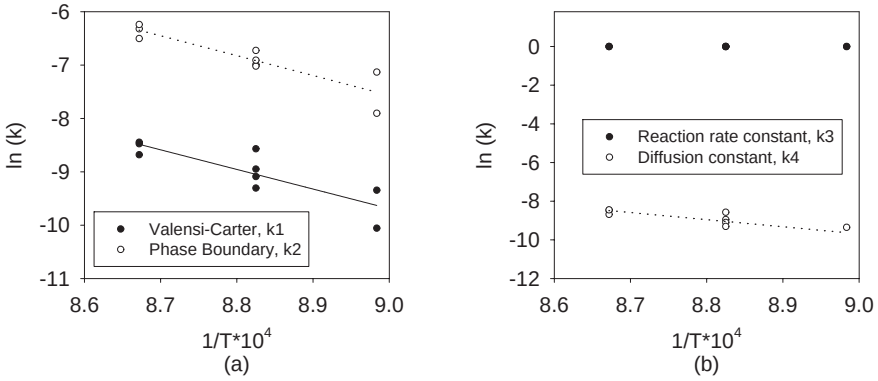

Figure 5.11. Arrhenius plots for experiments with 5% CO_2 in the inlet gas based on (a) the Valensi-Carter constant, k_1 ($\mu m^2/s$), and the phase boundary constant, k_2 ($\mu m/s$) and (b) the reaction rate constant, k_3 ($\mu m/s$), and the diffusion constant, k_4 ($\mu m^2/s$), for the modified shrinking-core model.

Table 5.4 shows the Arrhenius parameters for the experiments with carbon dioxide in the inlet gas. These results can also be compared with Table 5.3, i.e. the Arrhenius parameters for the experiments without carbon dioxide. The Valensi-Carter model has highest activation energy for experiments with 2% CO_2 and lowest with 0.5% CO_2. For the phase boundary model, experiments with 0% and 0.5% CO_2 show lower activation energy than experiments with 2% and 5%. The diffusion constant in the modified shrinking-core model is calculated at 2% and 5% CO_2 and show lower activation energy at 5% CO_2.

Table 5.4. Arrhenius parameters for the experiments with 0.5%, 2% and 5% carbon dioxide in the inlet gas.

	Pre-exponential factor, A	Activation energy, E (kJ/mol)
0.5% CO_2		
Valensi-Carter	$6.63 \cdot 10^{-5}$ m²/s	255
Phase boundary	338 m/s	250
Modified shrinking-core		
Reaction rate constant	-	-
Diffusion constant	-	-
2% CO_2		
Valensi-Carter	0.703 m²/s	345
Phase boundary	$1.83 \cdot 10^{5}$ m/s	311
Modified shrinking-core		
Reaction rate constant	-	-
Diffusion constant	0.772 m²/s	345
5% CO_2		
Valensi-Carter	$1.43 \cdot 10^{-2}$ m²/s	289
Phase boundary	$1.83 \cdot 10^{5}$ m/s	310
Modified shrinking-core		
Reaction rate constant	-	-
Diffusion constant	$1.55 \cdot 10^{-2}$ m²/s	306

Altogether, if fitting the models in the whole conversion interval, the reaction is controlled by diffusion mechanism at 840°C and by chemical kinetics at 860°C and 880°C for experiments with 0.5% CO_2. At 1% CO_2, the reaction is most probably controlled by diffusion at 860°C and by chemical kinetics at 880°C. At 2% CO_2 and 5% CO_2, diffusion seems to be the rate-determining mechanism in the whole temperature interval (840-880°C). A tendency can be seen that the reaction is controlled by diffusion instead of chemical kinetics at higher temperatures if the carbon dioxide concentration in the reaction atmosphere is increased.

However, it is important to keep in mind that although reasonably good standard deviations between experimental data and fitted models could be obtained, none of the models could give a good visual description of the reaction kinetics in the whole conversion interval. Moreover, the phase boundary model describes the experimental data well or very well for all experiments with carbon dioxide up to a conversion degree of 70-80%, which indicates that the reaction is controlled by chemical kinetics up to a conversion degree of 70-80%. This result is somewhat in contrast with what was seen from Table 5.2, Figures 5.9-5.11 and Appendix B (Table B.2-B.5), and consequently this is something that needs further investigations.

6 CONCLUSIONS

It was found for all amounts of carbon dioxide in the inlet gas that higher temperatures decrease the reaction time needed to reach complete conversion. The fact that there was some carbon dioxide in the inlet gas resulted in longer reaction times, though no clear differences were seen for different amounts of carbon dioxide.

X-ray diffraction (XRD) analysis showed that unreacted sodium trititanate and the product sodium pentatitanate were found in all samples. For the experiments without carbon dioxide, sodium metatitanate was found as well but not for the experiments without carbon dioxide, which is consistent with earlier findings by Zou (1991). This might explain that the samples without carbon dioxide sinter more than samples with carbon dioxide, since sodium metatitanate has a lower melting point than sodium trititanate and sodium pentatitanate.

Three different kinetic models were used to describe the experimental data; a diffusion controlled model, a chemical reaction rate controlled model and a model controlled by both diffusion and chemical reaction rate. When fitting the models to the experimental data, different results were obtained depending on the amount of carbon dioxide in the inlet gas. For the experiments without carbon dioxide in the inlet gas, the change from diffusion controlled to reaction rate controlled kinetics occurred around 820°C. At 800°C, the results showed that the reaction rate is controlled by diffusion and at 840-880°C by chemical reaction rate.

For experiments with 0.5% CO_2 in the inlet gas, the reaction rate is controlled by diffusion mechanism at 840°C and by chemical kinetics at 860°C and 880°C. With 1% CO_2 in the inlet gas, the reaction seems to be controlled by diffusion at 860°C and by chemical kinetics at 880°C. For experiments with 2% and 5% CO_2, diffusion seems to be the rate-controlling mechanism in the whole temperature interval (840-880°C). A tendency can be seen that the reaction is controlled by diffusion instead of chemical kinetics at higher temperatures if the carbon dioxide concentration in the reaction atmosphere is increased. However, it is important to keep in mind that none of the models could give a good visual description in the whole conversion interval when there were carbon dioxide in the reaction atmosphere. When the phase boundary model was fitted to the experimental data in the conversion range 8-73%, it could describe the data well or very well, which indicate that the reaction is controlled by chemical kinetics in the beginning of the reaction. It might then be expected that the reaction at higher conversion degrees, i.e. when the product shell has grown thicker, would show diffusion controlled reaction rate. This has not been confirmed in this investigation and consequently this is something that needs further investigations.

7 NOMENCLATURE

A = pre-exponential factor in the Arrhenius expression for k (m^2/s or m/s)
A_1 = inner surface area of the particle (m^2)
c = concentration (mol/m^3)
D_{eff} = effective diffusion coefficient (m^2/s)
E = the Arrhenius activation energy (J/mol)
k_1 = the Valensi-Carter rate constant (m^2/s)
k_2 = the phase boundary rate constant (m/s)
k_3 = a constant related to the first order reaction rate (m/s)
k_4 = a constant related to the lumped diffusivity (m^2/s)
k_r = first order reaction rate constant (m/s)
n = amount of diffusing compound (mol)
r_0 = initial radius of the sphere (m)
r_1 = instantaneous radius of reactant (m)
r_2 = instantaneous total radius (reacted and unreacted) of the sphere (m)
R = gas constant (8.3145 J/mol,K)
t = time (s)
T = temperature (°C)
x = degree of conversion (-)
z = volume of product formed per volume reactant consumed (m^2/m^3)
η = first-order reaction rate (mol/s)
ρ_{mA} = molar density of reactant A (mol/m^3)

8 REFERENCES

Andersson, S. and Wadsley, A.D., (1961), "The Crystal Structure of $Na_2Ti_3O_7$", *Acta Cryst.*, **14**, p.1245-1249.

Backman, R. and Salmenoja, K., (1994), "Equilibrium Behaviour of Sodium, Sulfur and Chlorine in Pressurized Black Liquor Gasification with Addition of Titanium Dioxide", *Paperi ja Puu – Paper and Timber*, **76**(5), p.320-325.

Carter, R.E., (1961), "Kinetic Model for Solid-State Reactions", *The Journal of Chemical Physics*, **34**(6), p.2010-2015.

Hanson, C., (1993), "Lime Mud Reburning – Properties and Quality of the Lime Produced", PhD Thesis, Chalmers University of Technology, Gothenburg, Sweden.

"Index to the Powder Diffraction File" (D5000 powder diffractometer of Siemens), File No. 31-1329, 37-345 and 28-1155.

Jander, W., (1927), "Reactions in Solid State at High Temperatures: I" (in German), *Z. Anorg. Allgem. Chem.*, **163**, p.1.

Kiiskilä, E., (1979), "Recovery of Sodium Hydroxide from Alkaline Pulping Liquors by Smelt Causticizing, Part II, Reactions between Sodium Carbonate and Titanium Dioxide", *Paperi ja Puu - Papper och Trä*, **61**(5), p.394-401.

Lindman, N. and Simonsson, D., (1978), "On the Application of the Shrinking Core Model to Liquid-Solid Reactions", *Chemical Engineering Science*, **34**, p. 31-35.

Nohlgren, I., (1999), "Recovery of Kraft Black Liquor Using the Titanate Process – Kinetics of the Direct Causticization Reaction between Sodium Tri-Titanate and Sodium Carbonate", Licentiate Thesis, Luleå University of Technology, Luleå, Sweden.

Palm, M. and Theliander, H., (1997), "Kinetic Study of the Direct Causticization Reaction Involving Titanates and Titanium Dioxide", *Chemical Engineering Journal*, **68**, p. 87-94.

Takei, H., (1976), "Growth and Properties of $Na_8Ti_5O_{14}$ Crystals", *Journal of Materials Science*, **11**, p.1465-1469.

Tamhankar, S.S. and Doraiswamy, L.K., (1979), "Analysis of Solid-Solid Reactions: A Review", *AIChE Journal*, **25**(4), p.561-582.

Zeng, L. and van Heiningen, A.R.P, (1997), "Pilot Fluidized-Bed Testing of Kraft Black Liquor Gasification and its Direct Causticization with TiO_2", *Journal of Pulp and Paper Science*, **23**(11), p. J511-516.

Zeng, L. and van Heiningen, A.R.P, (1998), "Sulphur Distribution during Air Gasification of Kraft Black Liquor Solids in a Fluidized Bed of TiO_2 particles", *Pulp & Paper Canada*, **100**(6), p.58-63

Zou, X., (1991), "Recovery of Kraft Black Liquor Including Direct Causticization", PhD Thesis, Dept. of Chemical Engineering, McGill University, Montreal, Quebec, Canada.

APPENDIX A

Table A.1. Start values of carbon dioxide concentration in the inlet gas (vol-%).

	840°C	860°C	880°C
0.5 mol-%	mpm145 - 0.4095	mpm142 - 0.4104	mpm139 - 0.4003
	mpm146 - 0.4118	mpm143 - 0.4088	mpm140 - 0.4048
		mpm144 - 0.4094	mpm141 - 0.4045
1 mol-%		(mpm123 - 1.1033)	mpm129 - 1.1229
		(mpm124 - 1.1020)	mpm130 - 1.1214
		(mpm127 - 1.1035)	mpm131 - 1.1475
		mpm161 - 1.0674	
		mpm162 - 1.0713	
		mpm163 - 1.0695	
2 mol-%	mpm138 - 2.0640	mpm135 - 2.0598	mpm132 - 2.0615
		mpm136 - 2.0618	mpm133 - 2.0598
		mpm137 - 2.0616	mpm134 - 2.0598
		mpm164 - 2.1311	
		mpm165 - 2.1350	
		mpm166 - 2.1357	
5 mol-%	mpm154 – 5.0007	mpm151 - 4.9803	mpm147 - 4.9957
	mpm155 – 4.9975	mpm152 - 4.9880	mpm148 - 5.0013
		mpm168 - 4.9683	mpm149 - 5.0006
		mpm169 - 4.9670	

Table A.2. Mean values of the BET specific surface area and mean deviation for each set of conditions.

TEMPERATURE	BET (m^2/g) MEAN VALUE	MEAN DEVIATION	NUMBER OF TRIALS
0% CO_2			
800°C	0.547	0.084	7
820°C	0.583	0.030	6
840°C	0.537	0.040	4
860°C	0.536	0.079	3
880°C	0.669	0.024	3
0.5% CO_2			
840°C	0.637	0.064	2
860°C	0.729	0.061	3
880°C	0.854	0.065	3
1% CO_2			
860°C	0.968	0.019	3
880°C	0.861	0.144	3
2% CO_2			
840°C	0.935	-	1
860°C	1.007	0.093	6
880°C	0.844	0.090	3
5% CO_2			
840°C	0.592	0.108	2
860°C	0.820	0.230	4
880°C	0.844	0.075	3

Mean deviations are calculated as:

$$\text{Deviation} = \frac{\sum_{i=1}^{n} \left| x_{av,i} - x_{exp,i} \right|}{n}$$

where $x_{av,i}$ is the average BET surface area at the specified set of conditions, $x_{exp,i}$ is the surface area for each measurement and n is the number of measurements for which the calculation is made.

APPENDIX B

Table B.1. The numerical values of the rate constants for experiments with 0% CO_2 in the inlet gas, which are obtained from fitting the kinetic models to experimental data and used in the Arrhenius plots.

	Valensi-Carter	Phase Boundary	Modified shrinking-core	
	k_1 [μm²/s]	k_2 [μm/s]	k_3 [μm/s]	k_4 [μm²/s]
800°C				
mpm113	2.1400E-05	1.85E-04	50→	2.1302E-05
mpm114	3.7364E-05	2.80E-04	7.9332E-04	5.3799E-05
mpm115	3.6412E-05	2.65E-04	6.0508E-04	5.9844E-05
mpm125	2.8742E-05	2.15E-04	7.4838E-04	3.8339E-05
mpm173	4.5387E-05	3.30E-04	30→	4.5176E-05
mpm174	5.4432E-05	4.45E-04	30→	5.4178E-05
mpm175	4.7745E-05	3.70E-04	5.7124E-03	3.0297E-05
820°C				
mpm158	6.0550E-05	4.05E-04	4.5221E-04	5.0655E-04
mpm159	5.9828E-05	3.85E-04	3.9637E-04	200→
mpm160	8.2028E-05	5.50E-04	5.4118E-04	200→
mpm170	7.4014E-05	6.15E-04	20→	7.3671E-05
mpm171	1.0532E-04	7.32E-04	9.6792E-04	3.6815E-04
mpm172	8.2503E-05	5.55E-04	6.4065E-04	5.4537E-04
840°C				
mpm104	1.8927E-04	1.10E-03	1.2403E-03	50→
mpm105	1.9554E-04	1.20E-03	1.2768E-03	100→
mpm106	1.2596E-04	8.25E-04	8.2354E-04	70→
mpm126	1.2267E-04	8.15E-04	8.0176E-04	120→
860°C				
mpm107	2.8237E-04	1.70E-03	1.2595E-03	500→
mpm108	2.3905E-04	1.45E-03	1.5572E-03	500→
mpm109	2.6167E-04	1.65E-03	1.5446E-03	500→
880°C				
mpm110	3.7369E-04	2.20E-03	2.4171E-03	300→
mpm111	3.3956E-04	1.95E-03	1.3039E-03	300→
mpm112	3.3259E-04	2.10E-03	2.1482E-03	500→

Note: For the constants with "→", the fitting of the models to experimental data are almost independent of the value of the constant.

Table B.2. The numerical values of the rate constants for experiments with 0.5% CO_2 in the inlet gas, which are obtained from fitting the kinetic models to experimental data and used in the Arrhenius plots.

	Valensi-Carter	Phase boundary	Modified shrinking-core		Phase boundary 8-73%
	k_1 [µm²/s]	k_2 [µm/s]	k_3 [µm/s]	k_4 [µm²/s]	k_2 [µm/s]
840°C					
mpm145	7.00E-05	6.30E-04	1→	7.00E-05	7.40E-04
mpm146	7.70E-05	6.30E-04	1→	7.70E-05	7.20E-04
860°C					
mpm142	1.38E-04	1.15E-03	1.15E-03	1→	1.20E-03
mpm143	1.20E-04	1.05E-03	1.05E-03	1→	1.20E-03
mpm144	1.10E-04	9.60E-04	9.60E-04	1→	1.10E-03
880°C					
mpm139	1.90E-04	1.60E-03	1.60E-03	1→	1.80E-03
mpm140	1.87E-04	1.50E-03	1.50E-03	1→	1.60E-03
mpm141	1.97E-04	1.80E-03	1.80E-03	1→	1.80E-03

Table B.3. The numerical values of the rate constants for experiments with 1% CO_2 in the inlet gas, which are obtained from fitting the kinetic models to experimental data and used in the Arrhenius plots.

	Valensi-Carter	Phase boundary	Modified shrinking-core		Phase boundary 8-73%
	k_1 [µm²/s]	k_2 [µm/s]	k_3 [µm/s]	k_4 [µm²/s]	k_2 [µm/s]
860°C					
mpm161	1.05E-04	9.25E-04	1→	1.05E-04	1.05E-03
mpm162	9.35E-05	8.40E-04	1→	9.35E-05	1.00E-03
mpm163	9.60E-05	8.45E-04	1→	9.60E-05	1.00E-03
880°C					
mpm129	1.99E-04	1.70E-03	1.70E-03	1→	1.80E-03
mpm130	1.71E-04	1.40E-03	1.40E-03	1→	1.55E-03
mpm131	2.05E-04	1.65E-03	1.65E-03	1→	1.60E-03

Table B.4. The numerical values of the rate constants for experiments with 2% CO_2 in the inlet gas, which are obtained from fitting the kinetic models to experimental data and used in the Arrhenius plots.

	Valensi-Carter	Phase boundary	Modified shrinking-core		Phase boundary 8-73%
	k_1 [μm²/s]	k_2 [μm/s]	k_3 [μm/s]	k_4 [μm²/s]	k_2 [μm/s]
840°C					
mpm138	5.35E-05	5.00E-04	1→	5.35E-05	7.00E-04
860°C					
mpm135	1.06E-04	9.20E-04	1→	1.06E-04	1.03E-03
mpm136	8.80E-05	7.80E-04	1→	8.80E-05	9.00E-04
mpm137	8.55E-05	8.10E-04	1→	8.55E-05	1.00E-03
mpm164	8.20E-05	7.65E-04	1→	7.96E-05	9.00E-04
mpm165	8.85E-05	8.30E-04	1→	8.85E-05	9.50E-04
mpm166	8.18E-05	7.95E-04	1→	8.19E-05	1.00E-03
880°C					
mpm132	2.10E-04	1.75E-03	1→	2.10E-04	1.90E-03
mpm133	1.79E-04	1.50E-03	1→	1.79E-04	1.70E-03
mpm134	1.56E-04	1.35E-03	1→	1.56E-04	1.57E-03

Table B.5. The numerical values of the rate constants for experiments with 5% CO_2 in the inlet gas, which are obtained from fitting the kinetic models to experimental data and used in the Arrhenius plots.

	Valensi-Carter	Phase boundary	Modified shrinking-core		Phase boundary 8-73%
	k_1 [μm²/s]	k_2 [μm/s]	k_3 [μm/s]	k_4 [μm²/s]	k_2 [μm/s]
840°C					
mpm154	8.75E-05	8.00E-04	1→	8.70E-05	1.20E-03
mpm155	4.30E-05	3.70E-04	1→	4.30E-05	4.70E-04
860°C					
mpm151	1.30E-04	1.20E-03	1→	1.30E-04	1.65E-03
mpm152	1.13E-04	9.20E-04	1→	1.12E-04	9.50E-04
mpm168	9.11E-05	8.95E-04	1→	9.12E-05	1.23E-03
mpm169	1.60E-04	1.00E-03	1→	1.90E-04	2.60E-03
880°C					
mpm147	2.09E-04	1.80E-03	1→	2.09E-04	2.10E-03
mpm148	1.70E-04	1.50E-03	1→	1.70E-04	1.80E-03
mpm149	2.15E-04	1.95E-03	1→	2.15E-04	2.10E-03